JET–P(98)51

D F H Start et al

Bulk Ion Heating with ICRH in JET D–T Plasmas

JET–P(98)51

Bulk Ion Heating with ICRH in JET D–T Plasmas

D F H Start[+], J Jacquinot, V Bergeaud[1], V P Bhatnagar, S Conroy[2], G A Cottrell, S Clement, G Ericsson[2], L–G Eriksson, A Fasoli[3], V Fuchs[4], A Gondhalekar, C Gormezano, G Gorini[5], G Grosshoeg[6], K Günther, P Harbour, R F Heeter[7], L D Horton, A Howman, H J F Jäckel, O N Jarvis, J Källne[2], C N Lashmore-Davies[8], K D Lawson[8], C Lowry, M Mantsinen[9], F B Marcus, R Monk, E Righi[10], F G Rimini, G J Sadler, G R Saibene, R Sartori, B Schunke, S Sharapov, A C C Sips, M Stamp, M Tardocchi[2], P van Belle.

JET Joint Undertaking, Abingdon, Oxfordshire, OX14 3EA, UK,
[+]Suddenly passed away on 14 August 1998, a month after completing this manuscript.
[1]DRFC, Association Euratom-CEA, CEN Cadarache, 13108 Saint-Paul-Lez-Durance, France.
[2]Department of Neutron Research, Uppsala University, S-75121 Uppsala, Sweden.
[3]Plasma Science and Fusion Centre, MIT, Cambridge, MA 02139, USA.
[4]Centre Canadien de Fusion Magnetique, Varennes, Quebec, J3X 1S1, Canada.
[5]INFM, Physics Department, Milano University, Milano, Italy, and "Piero Caldirola" Inst. of Plasma Physics, CNR, Milano, Italy.
[6]Chalmers University of Science and Technology, S-41296, Gothenburg, Sweden.
[7]Princeton Plasma Physics Laboratory, Princeton, New Jersey, USA.
[8]UKAEA Fusion, UKAEA/Euratom Fusion Association, Culham, Oxfordshire, OX14 3DB, UK.
[9]Also at Helsinki University of Technology, Association Euratom–Tekes, 02150 Espoo, Finland.
[10]The NET Team, IPP, 85478 Garching, Germany.

Preprint of a Paper to be submitted for publication in Nuclear Fusion

December 1998

ABSTRACT.

Reactor relevant ICRH scenarios have been assessed during D-T experiments on the JET tokamak using H-mode divertor discharges with ITER-like shapes and safety factors. Deuterium minority heating in tritium plasmas was demonstrated for the first time. For 9% deuterium, an ICRH power of 6 MW gave 1.66 MW of fusion power from reactions between suprathermal deuterons and thermal tritons. The Q-value of the steady state discharge reached 0.22 for the length of the RF flat top (2.7 s), corresponding to three plasma energy replacement times. The Doppler broadened neutron spectrum showed a deuteron energy of 125 keV which was optimum for fusion and close to the critical energy. Thus strong bulk ion heating was obtained at the same time as high fusion efficiency. Deuterium fractions around 20% produced the strongest ion heating together with a strong reduction of the suprathermal deuteron tail. The edge localised modes (ELMs) had low amplitude and high frequency and each ELM transported less plasma energy content than the 1% required by ITER. The energy confinement time, on the ITERH97-P scale, was 0.90 which is sufficient for ignition in ITER. He^3 minority heating, in approximately 50:50 D:T plasmas with up to 10% He^3, also demonstrated strong bulk ion heating. Central ion temperatures up to 13 keV were achieved together with central electron temperatures up to 12 keV. The normalised H-mode confinement time was 0.95. Second harmonic tritium heating produced energetic tritons above the critical energy. This scheme heats the electrons in JET unlike in ITER where the lower power density will allow mainly ion heating. The inverted scenario of tritium minority ICRH in a deuterium plasma was demonstrated as a successful heating method producing both suprathermal neutrons and bulk ion heating. Theoretical calculations of the D-T reactivity mostly give excellent agreement with the measured reaction rates.

1. INTRODUCTION

The ion cyclotron resonance heating (ICRH) system on JET has been designed to operate with a wide range of fundamental and multiple harmonic scenarios [1]. The frequency band covers the range 23 MHz to 56 MHz and the system has coupled up to 22.3 MW of power to the plasma using four antennas [2]. Each of the present antennas has four current straps and the phase difference between currents in adjacent straps can be set at any desired value. The results described in this paper were obtained with a phase difference of π (except for those in Fig 11). The versatility of the system was exploited in the recent JET experiments with D-T plasmas which provided a unique opportunity to assess the physics and performance of ICRH schemes that are relevant to a reactor. These schemes comprise He^3 and deuterium minority ions at their fundamental resonances and tritium majority ions at their second harmonic resonance. The He^3 and second harmonic tritium schemes were used in both tritium dominated and approximately 50:50 D:T plasmas. In the deuterium minority scheme the deuterium fraction varied between 9% and 22%. In addition, tritium minority heating experiments were carried out with 5% tritium in 95% deuterium plasmas. The frequency range necessary for these studies ranged from 23 MHz for

the tritium minority to 37 MHz for the He^3 fundamental and tritium second harmonic scenarios. In most cases the resonance was placed on the magnetic axis. However, for the tritium minority experiments the lowest frequency of the ICRH plant, and the highest magnetic field (B_T = 3.9T including paramegnetic effect), only allowed the resonance to be on the high field side, some 0.4m from the plasma centre. The experiments were carried out in H-mode plasmas, except for the tritium minority studies where the power was below the H-mode threshold. The plasma shapes were similar to that of ITER with edge safety factors in the range $3.4 < q_{95} < 3.9$. The JET divertor, RF antennas, poloidal limiters and shape of a typical discharge are shown in Fig. 1.

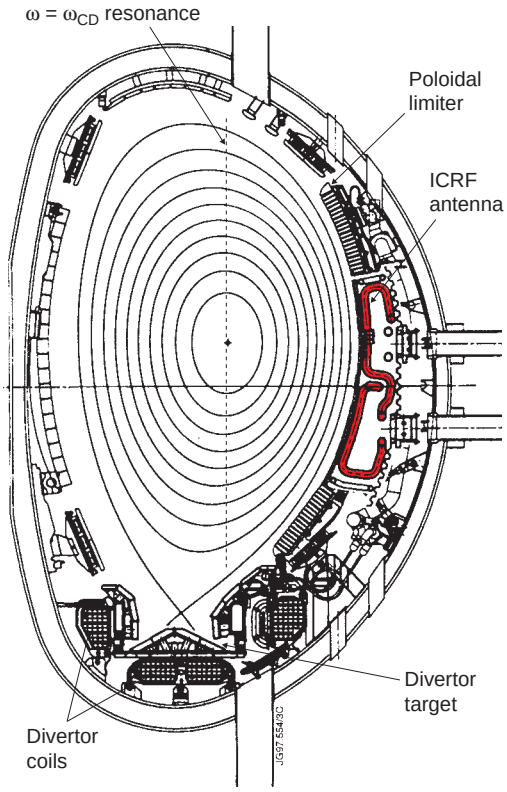

Fig. 1. Cross section of JET showing flux surfaces for a single null divertor discharge typical of the present experiments.

Between 23 MHz and 37 MHz the antenna loading changes by a factor of two with the smallest loading at the lowest frequency (typically 0.7 Ω at 23 MHz). This decrease is due to the antenna being resonant at around 45 MHz together with the characteristic impedance of the antenna straps being less [3] than the 30 Ω of the feed lines. In this loading range (0.7 Ω to 1.5 Ω including the vacuum loading of about 0.5Ω) the power coupled to the plasma is determined by the voltage sustainable on the antenna and its supply lines. The D-T campaign provided a long period of continuous conditioning which enabled operating voltages up to 35 kV to be achieved.

For the minority scenarios, operation in tritium and D-T plasmas significantly improves the single pass absorption fraction compared with operation in deuterium. The reason is that the left hand circularly polarised electric field component is enhanced by, typically, 50% in tritium plasmas. The ratio of the left to the right hand polarisation (E_+/E_-) is given [4] by $[(Z/A)_m - (Z/A)_M]/[(Z/A)_m + (Z/A)_M]$ where Z and A are the atomic number and mass of the ions and the subscripts m and M denote the minority and majority species, respectively. Table 1 shows the polarisation ratios for several scenarios in D and T plasmas. Most notable for the present experiments is the improvement for the He^3 minority case which reduces both direct electron absorption and the cross talk between antennas in discharges with low single pass damping.

In the next section, the results of the deuterium minority experiments are described. This scenario gives strong bulk ion heating and a record Q-value for a steady state discharge. The He^3 minority and the tritium second harmonic resonances occur at the same magnetic field for a

Table 1. Ratio of left to right hand polarisation for minority ICRH schemes (cold plasma theory).

Scenario	**E_+/E_-**
(H) – T	0.5
(H) – D	0.33
(He^3) – T	0.33
(He^3) – DT (50%)	0.25
(D) – T	0.20
(He^3) – D	0.14

given frequency and are competing mechanisms for absorption of the fast wave. The results of experiments in which one or other of these mechanisms dominates, with a range of He^3 concentrations up to 10%, are given in section 3. Bulk ion heating is observed when the damping is by the He^3 ions; when the tritium second harmonic absorption dominates, mainly electron heating occurs. The investigation of the tritium minority scheme which generates neutrons from suprathermal reactions together with ion heating is presented in section 4. A summary of the results and their implications for ITER is given in section 5.

2. FUNDAMENTAL DEUTERIUM MINORITY HEATING.

The potential of the deuterium minority ICRF scenario for both plasma heating and for generating fusion power through suprathermal reactions has been recognised for a number of years [4, 5]. Theoretical calculations for ITER [6] suggest that, with $k_{//} \approx 4\ m^{-1}$, deuterium concentrations around 30% will provide maximal bulk ion heating. For higher deuterium fractions, direct electron damping will become a strong competitor to the deuterium cyclotron absorption. For JET conditions, theory predicted that a deuterium concentration between 10% and 20% would produce maximum suprathermal reactivity [5, 7]. In the JET D-T campaign described here, the deuterium minority ICRH scheme was tested and optimised for the first time. The experiments were carried out at a frequency of 28 MHz and a toroidal magnetic field of 3.7 T to give central RF power deposition. Power levels up to 6 MW were used and the plasma current was either 3.3 MA or 3.7 MA. The highest performance achieved with this scenario is described in the next section. In section 2.2 the results of varying the deuterium concentration between 9% and 22% are discussed.

2.1 Maximum fusion reactivity.

The fusion reactivity between the suprathermal deuterons and the thermal tritons was maximised by achieving an average deuteron energy close to 120 keV, the energy at which the D-T rate coefficient peaks. This was attained by varying the central density, n_{eo}, in the range $3.3 \times 10^{19}\ m^{-3}$ to $5.0 \times 10^{19}\ m^{-3}$ and the deuterium concentration in the range 9% to 22%. As reported in reference 8, the best results were obtained at an ICRF power of 6 MW, a D:T ratio of

9:91 and a density of 5.0×10^{19} m^{-3}. The fusion power reached 1.66 MW and the steady state fusion figure of merit, $Q = P_{fus}/(P_{RF} + P_{OH})$, was 0.22 over a period of 2.7s (three energy replacement times). The parameters P_{fus}, P_{RF} and P_{OH} are the output fusion power, the input RF power and the ohmic heating power, respectively. The period of 2.7s was limited by neutron economy. The time evolution of the fusion power is shown in Fig. 2. An H-mode is produced at 13.7 s as can be seen from the appearance of edge localised modes (ELMs) which are detected as sharp, transient increases in the deuterium and tritium Balmer-α light (D_α + T_α). The frequency of these small amplitude ELMs is about 250 Hz. The ratio of the ELM repetition time and the confinement time (0.87s) gives an upper limit of 0.5% to the fraction of the plasma energy content (ΔW/W) transferred by each ELM across the scrape-off layer. This value is less than that required by ITER (1%) to prevent excessive wall erosion [9]. The energy confinement time, τ_E = 0.87 s, corresponds to an ELMy H-mode quality factor, ITERH97-P, of 0.90 which will allow ignition on ITER [10].

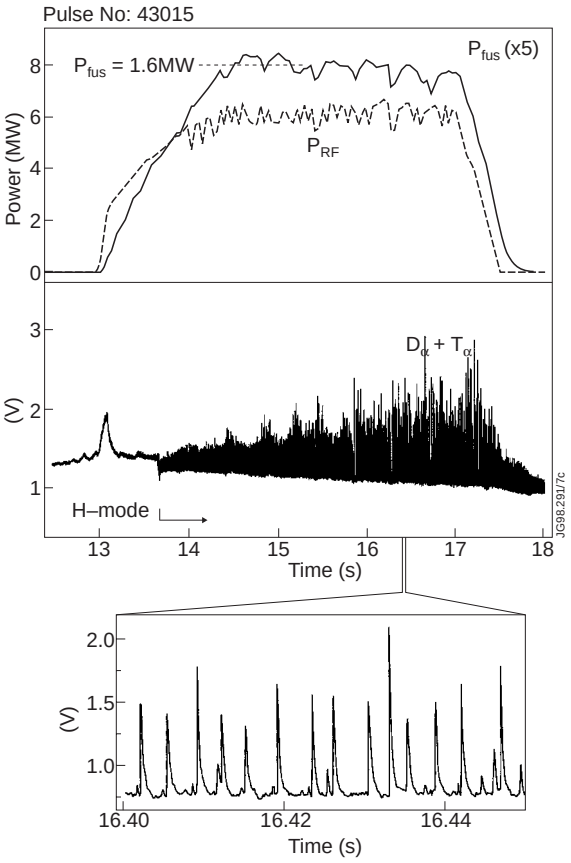

Fig. 2. Fusion power from the best (D)T minority heating discharge with I_p = 3.7 MA and B_T = 3.7 T. Inset is an expanded view of the ELMs which had small amplitude and an average frequency of 250Hz.

The ion and electron temperature profiles measured by charge exchange spectroscopy (CXS) and electron cyclotron emission (ECE), respectively are shown in Fig. 3. These data are taken during the flat top of the 0.4 s long sawteeth. In general the CXS diagnostic used two tritium neutral beams at a total power level of 2.3 MW to give sufficient signal from the plasma centre and to provide redundancy against failure. In a few cases, data were also recorded with a single beam to be sure that the beams themselves were not producing significant ion heating and thus distorting the measurement. Identical values of T_i were obtained at both diagnostic NBI power levels. In figure 3 the

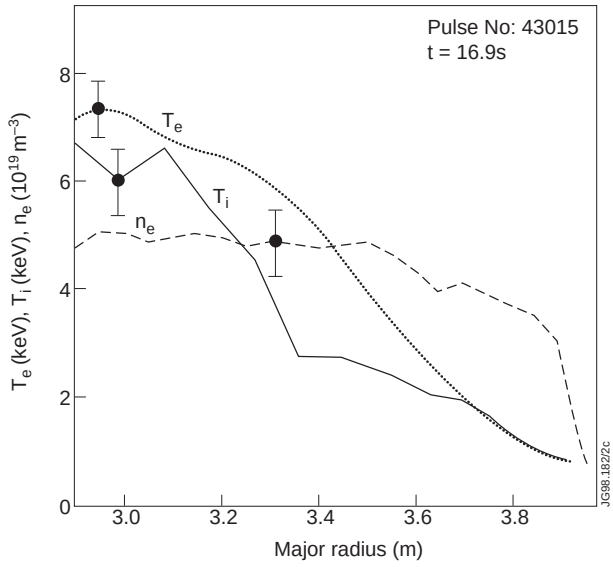

Fig. 3. Temperature and density profiles for the discharge shown in figure 2.

central ion temperature (T_{io} = 6.6 ± 0.6 keV) is close to the central electron temperature, T_{eo} = 7.2 ± 0.4 keV showing the presence of substantial bulk ion heating by the deuterons. Such ion heating is expected since the deuteron energy (E_{crit}) which gives equal collisional power transfer to the ions and electrons is 100 keV for an electron temperature of 7 keV [11]. Detailed theoretical calculations using the PION code [12] for discharge 43015 are given in references 8 and 13. The calculation contains no free parameters and self-consistently treats the evolution of the fast ion distribution and power absorption. Redistribution of the fast ions by sawteeth, as observed experimentally [8], is also included. The predicted fusion reactivity is in excellent agreement with the observed reactivity [13]. The power partition calculations predict that 70% of the power is absorbed by the deuterons, 15% by carbon plus beryllium impurities, 10% by direct electron damping and 5% by mode conversion. The direct electron absorption occurs through a combination of transit time magnetic pumping (TTMP) and electron Landau damping (ELD). Summing the components, including the ohmic heating, gives a ratio of ion to electron heating of 45:55 which is consistent with T_{io} slightly less than T_{eo}. The α-particle concentration is not accurately known but it is estimated to be about 0.01% in the JET ICRH experiments. PION code calculations show that at such a low concentration, the power absorbed by α-particles is below 0.2%.

The deuteron energy has been obtained from the Doppler broadening of the 14 MeV neutron energy spectrum and, for some discharges, from neutral particle analysis. The neutron data for discharge 43015 are given in reference 8 and show a deuteron energy of 125 ± 25 keV. The deuteron velocity distribution given by the neutral particle analyser, NPA, for discharge 42792, which produced 1.2 MW of fusion power with an RF power of 4.7 MW, is shown in Fig. 4. The fast particle NPA [14] measures in the energy range 0.3 MeV to 1.1 MeV. The tail temperature is about 96 keV which is in good agreement with the neutron spectroscopy measurement of 100 keV for this discharge (see Fig. 7).

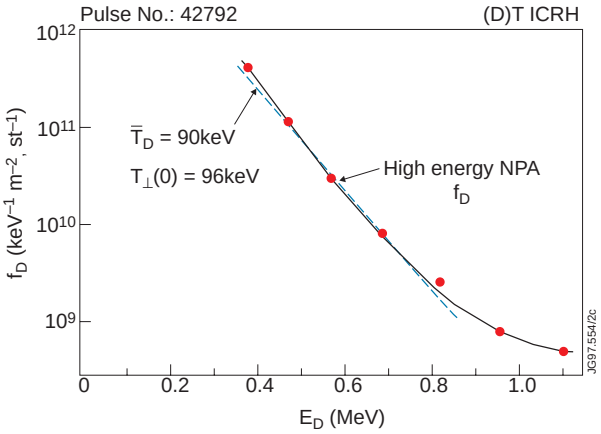

Fig. 4. Line integral deuteron distribution function obtained from the NPA for discharge 42792 (I_p = 3.7 MA, B_T = 3.7 T) which produced 1.2 MW of fusion power for 4.7 MW of ICRF power. The inferred tail temperature at the plasma centre, $T_\perp(0)$ is 96 keV.

2.2 Variation of the deuterium concentration

During the search for highest fusion reactivity, the deuterium fraction was varied between 9% and 22% of the total ion density. The fusion yield was highest at 9% but the highest central ion temperatures, and the strongest ion heating, occurred at the larger concentrations. At these concentrations there is substantial evidence for a transfer of power absorption away from the suprathermal deuterons towards a strong central bulk ion heating scheme.

The first evidence came from PION code calculations which overestimated the neutron emission for high deuterium fractions [13]. To reproduce the observed neutron rate it was necessary to reduce, artificially, the power in the fast wave to 40% of the input power. In contrast, calculations for all discharges with about 10% minority concentration require no such reduction in fast wave power to reproduce the observed D-T reactivity. The experimental data support this reduction of fast wave power to the deuterons but also show that all the power is deposited in the plasma core with a large fraction flowing to thermal ions.

These data are discussed below along with candidate heating mechanisms. Perhaps the most likely of these is mode conversion to an ion Bernstein wave (IBW) which is absorbed by cyclotron damping on thermal deuterons. Ion damping of an IBW has been observed in supershots in the TFTR tokamak [15], although the TFTR experiments had a higher deuterium fraction and the damping occurred on the tritons.

The highest value of T_{io} was achieved with 18% deuterium fraction, an electron density of 3.4×10^{19} m^{-3} and 4.8 MW of ICRF power . In this discharge, 42769, for which the plasma current was 3.3 MA, T_{io} reached 10.5 keV compared with a central electron temperature of 8.3 keV as shown in Fig. 5. For comparison, the characteristics of a discharge 42792 (I_p = 3.7 MA) with the same RF power but with 10% deuterium and $n_{eo} = 4.6 \times 10^{19}$ m^{-3} is also shown. In this case, T_{eo} was 7.5 keV and T_{io} reached only 6.2 keV even though the confinement times were almost identical in the two discharges. The profiles of ion and electron energy densities are shown in Fig 6. The ion energy density is greatest for the 18% deuterium case and is the same as the electron energy density for the 10% deuterium discharge. Furthermore, the total thermal energy contents, and their radial profiles are almost identical in the two cases which implies that the

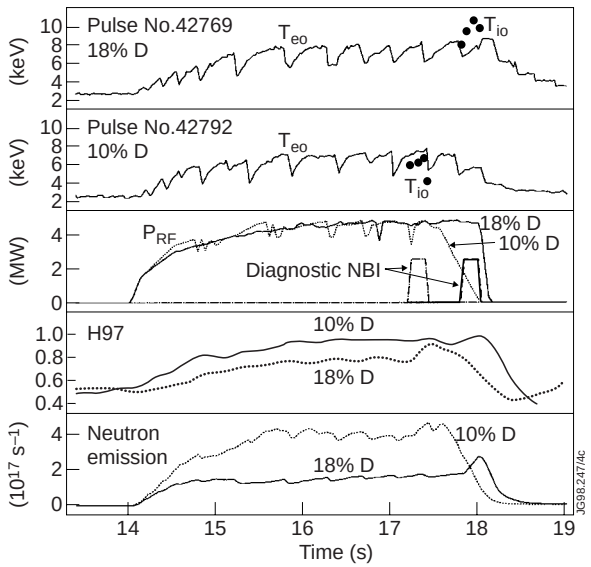

Fig. 5. Comparison of discharges with 10% deuterium (42792) and an increasing deuterium fraction up to 18% (42769). The evolution of the deuterium concentration for 42769 can be seen in figure 8.

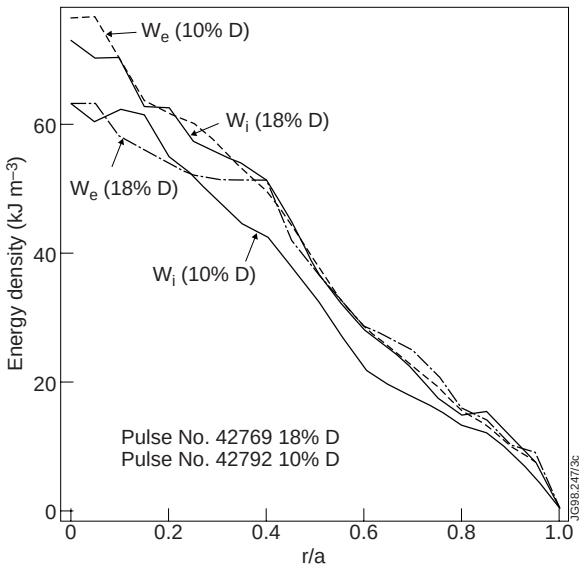

Fig.6. Ion and electron energy contents for 10% and 18% deuterium minority fractions. Note that the ion energy content of each discharge is similar to the electron energy content of the other.

ICRF power deposition is the same for each discharge, and predominantly in the plasma core. Since the thermal energy contents are similar, the higher current and density in the 10% deuterium case results in a lower normalised confinement ($\tau_{ITERH97\text{-}P} \propto I_p^{0.9}.n_e^{0.4}$); H97 = 0.8 compared with H97 = 0.95 for the 18% deuterium case, as can be seen in Fig. 5.

The combination of higher minority concentration and reduced fast wave power absorption produces a striking reduction of the deuterium average energy as can be seen from the Doppler broadened neutron spectra in Fig 7. These data were obtained with the proton recoil spectrometer, 'Tansy', [16] which has a narrow vertical line of sight through the plasma centre. The broadening detected by the instrument is mainly due to the gyro-motion of the fast deuterons. The spectra shown in Fig. 7 are the integrated counts throughout the RF pulse excluding the period occupied by the diagnostic beams. The results for the 10% and 18% minority discharges, respectively, are the top and bottom traces in Fig. 7; an intermediate example (13% deuterium) is shown in the centre of the figure. The data are modelled with a deuterium distribution comprising an anisotropic Maxwellian with perpendicular and parallel temperatures $T_\perp$ and $T_{//}$, respectively, together with an isotropic thermal Maxwellian component with the measured value of T_i. A thermal distribution is used for the tritons. The response of the spectrometer is calculated with a Monte Carlo code for a range of values of $T_\perp$, $T_{//}$, and the magnitude of the thermal deuteron component. The best values of the parameters are then determined from a χ^2 fit to the data. The results of this process are shown in Fig 7. For the 10% deuterium fraction the suprathermal reactions dominate and the deuteron tail temperature is 100 keV in agreement with the NPA measurement (Fig 4). For the 18% deuterium fraction the thermal reactivity contributes 60% of the total. This value, derived from the least square fit, agrees well with the value of 53% calculated from the ion temperature and density profiles measured at 17.9sec (Fig. 5).

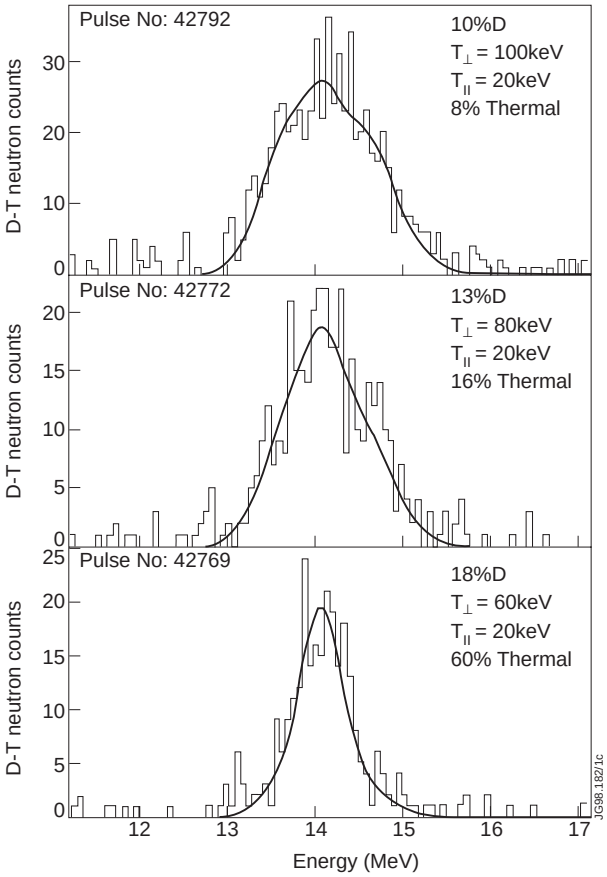

Fig. 7. Neutron energy spectra for (D)T ICRH Doppler broadened by the velocity of the deuterons. The solid curves are best fits to the data of a combination of suprathermal and thermal components.

The time dependent changes in the deuteron velocity distribution are revealed in the neutron spectra recorded with the MPR (magnetic proton recoil) spectrometer [17]. The MPR is placed close to the tokamak, viewing the plasma along a nearly horizontal line of sight making

a double pass through the plasma centre. It operates at high count rate which made it possible to measure the width of the neutron emission spectrum for discharge 42769 with about 30 ms time resolution (Fig. 8). The instrumental energy resolution is 23mm (FWHM) for a dispersion of 12.7 mm per ΔE/E = 1%.

Also shown in Fig. 8 are the deuterium fraction, which rises from 11% to 18%, and the central neutron emissivity from the neutron profile monitor [18]. As the ICRF power is ramped up, the perpendicular temperature of the deuterons increases to about 80 keV. However, at 15.2 s, coincident with the crash of a monster sawtooth, the deuterium energy begins to fall. By 17 s the spectrum is consistent with thermal distributions of deuterons and tritons of 15 keV. This is higher than the measured ion temperature (10.5 keV) indicating the presence of a remnant suprathermal deuteron population. At 15.8 s there appears to be a partial recovery which is curtailed by the crash of another monster sawtooth. Note also, from Fig. 5, the shortening of the sawteeth after 16 s as the stabilising effect [19] of the fast ion pressure reduces.

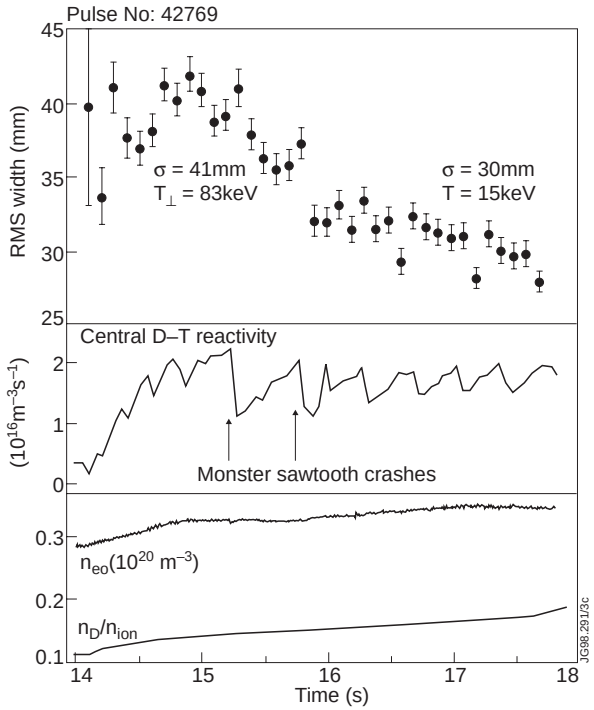

Fig. 8. The measured time evolution of the width, σ, of the neutron emission spectrum for discharge 42769 from which is deduced $T_\perp$ = 83 keV for RF accelerated deuterons at the beginning of the RF pulse (t = 15.3 s) and T_i = 15 keV (the effective average value for t > 16 s). The spectrometer energy dispersion is 12.7 mm (along the focal plane of the magnet) per ΔE/E = 1%.

To summarise, at minority fractions around 20% both the experimental data and the D-T reaction rate simulations suggest that a large fraction of the fast wave power is not cyclotron damped by the deuterons. However, this power fraction still produces strong thermal ion heating in the plasma core. Possible mechanisms include mode conversion to an ion Bernstein wave, with subsequent damping by ions, or absorption of the fast wave by fully stripped Be^9 ions.

As remarked above, mode conversion followed by cyclotron damping of the IBW was seen in TFTR at high T_i. For the JET plasmas, ISMENE code calculations indicate that the mode converted power is of the order required. However, since the mode conversion surface is 0.2m on the high field side of the deuterium resonance, the IBW must propagate towards the low field side, counter to its usual direction, to be in cyclotron resonance with thermal deuterons. The poloidal field can strongly influence the propagation of these short wavelength electrostatic waves [20] and it has been shown that outward travelling waves can occur away from the equatorial plane of a discharge and damp on the minority ions [21].

Fully ionised Be^9 has its fundamental resonance close to the D-T ion-ion hybrid layer where the E_+ field is large. The beryllium also produces an ion-ion hybrid layer close to its cyclotron resonance which further enhances absorption. Discharge 42769 has Z_{eff} = 1.5 in the centre and the Be^9 concentration is about 1.5%. ISMENE code [22] simulations suggest that beryllium can absorb up to 40% of the power. The beryllium ions achieve about 20 keV energy so that the collisional power transfer is to the tritium and deuterium to produce strong bulk ion heating. However, this heating is ~ 0.35 m off-axis whereas the T_i profile is as peaked as that in Fig. 3 for central D-minority absorption. Furthermore, time dependent calculations cannot simulate the transition from damping on deuterons to beryllium once the deuteron tail is formed. Clearly, more experiments are needed to establish definitively which of the above mechanism is present. For example, the response of T_i to power modulation will reveal whether the ion heating profile is central or off-axis.

3. HE^3 MINORITY AND TRITIUM SECOND HARMONIC ICRH

3.1 High tritium fraction discharges

Fundamental He^3 minority and second harmonic tritium ($2\omega_{CT}$) ICRH are necessarily competing absorption mechanisms since both resonances occur at the same position in the plasma. He^3 minority in D-T plasma is a strongly absorbing scheme, according to table 1, with increasing single pass damping as the tritium fraction increases. The second harmonic tritium absorption relies on finite Larmor radius effects to allow damping of the fast wave. The single pass absorption is typically weaker than that for He^3 minority in JET plasmas. The first investigations in this campaign were carried out during tritium loading of the JET vessel walls which produced plasmas with up to 95% tritium fraction.

The key discovery was that a small amount of He^3, typically 2%, strongly enhances the neutron emission as illustrated in Fig. 9. The discharges shown had D:T = 10:90, a plasma current of 3 MA and a toroidal magnetic field of 3.4T. The ICRF frequency was 34 MHz which placed the resonances in the plasma centre. Discharge 41734 has no He^3 injection and the fast wave power is absorbed partly by tritons and partly by electrons (TTMP + ELD) according to PION calculations (see section 3.2, and ref. 13 for example). About 0.1% He^3 will be present in the tritium from radioactive decay and could absorb up to 30%

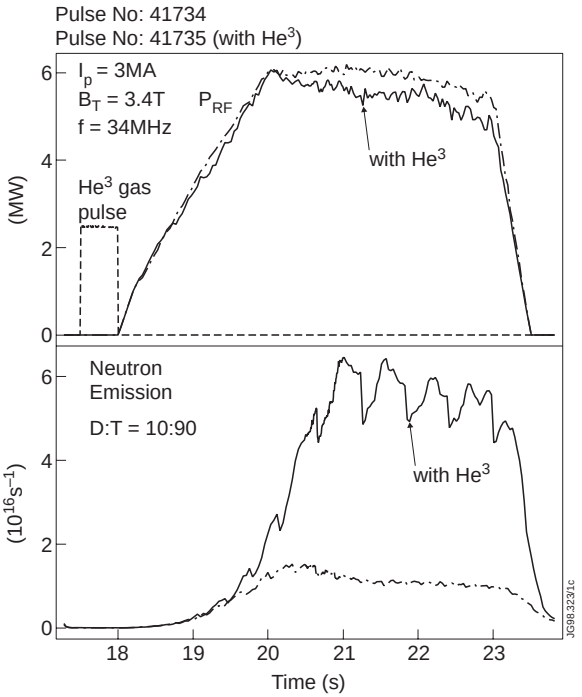

Fig. 9. Increased reactivity with 4% He^3 added to the second harmonic tritium ICRF scenario.

of the power in the absence of RF pump-out from the plasma centre. However, simulations of the neutron emission give best results for no power absorption by He^3 [13]. The neutron emission is $1.5x10^{16}$ s^{-1} for 6 MW of ICRH power. On the other hand, discharge 41735 has almost identical ICRF power but He^3 is injected prior to the application of the ICRH to give a concentration $n_{He3}/n_e \approx 4\%$. In this case the neutron emission is increased fourfold to $6.5x10^{16}$ s^{-1}. The crashes in the neutron flux correspond to monster sawtooth crashes. Increasing the He^3 beyond 4% produces no further improvement.

The higher reactivity with He^3 minority heating is due to the higher ion temperature. As can be seen from Fig 10, the value of T_i measured by X-ray crystal spectroscopy [23] at r/a = 0.43 is 5 keV for the He^3 case and 3 keV for the $2\omega_{CT}$ case. The density is also 30% higher in the former discharge ($n_{eo} = 2.7x10^{19}$ m^{-3} and $3.4x10^{19}$ m^{-3}, respectively, for discharges 41734 and 41735) so that the ion energy density is approximately a factor of two higher with He^3 minority heating. A precise comparison was not possible due to a lack of $T_i(r)$ profile data during these measurements. The central electron temperature is also larger in the He^3 minority case, mainly due to the monster sawteeth whose presence indicates a greater fast ion pressure inside the q = 1 surface. The H-mode factor reaches H97 = 1.1 and 0.75 with and without He^3 injection, respectively.

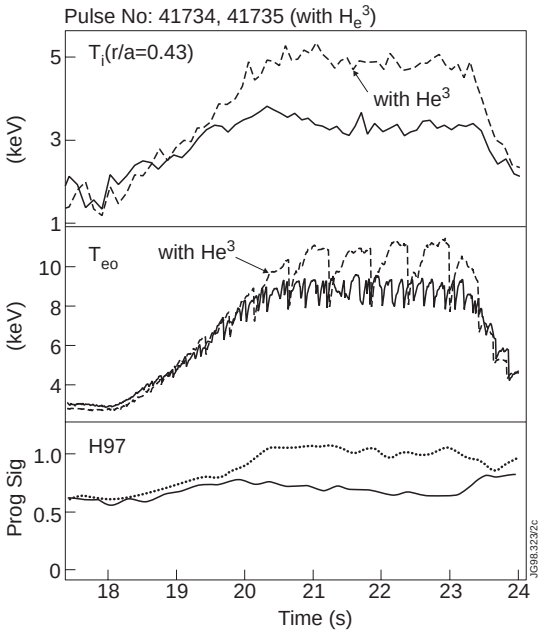

Fig. 10. Comparison of $2\omega_{CT}$ scenarios with and without He^3. Bulk ion heating increases when minority He^3 ICRH dominates. The lower H-factor with 'pure' $2\omega_{CT}$ heating is due to loss of tritons on large orbits and to orbit broadening of the heating profile.

The reduced H-factor with 'pure' $2\omega_{CT}$ heating is understood, at least in part, to be due to the large orbits of the tritons. PION calculations show that a small number of tritons are accelerated to MeV energies. Above 4 MeV some trapped particle orbits intersect the limiters and about 20% of the input power is lost in this way. Such loss is not included in the calculation of H97 and also reduces the power in excess of the H-mode threshold. In addition, the large triton orbits broaden the collisional heating profile which reduces the global confinement; the lack of monster sawteeth (Fig. 10) testifies to the broad fast ion density profile.

With He^3 injection, the greater ion heating is mainly due to two factors. The strong single pass absorption by the He^3 ions reduces the competing TTMP + ELD power flowing to the electrons, and the average energy of the He^3 ions is close to E_{crit} which is about 240 keV for discharge 41735. In contrast, the $2\omega_{CT}$ scheme accelerates the ions well above E_{crit} (Fig. 11). Similar distributions are seen with $2\omega_{CT}$ heating in TFTR [15]. The energetic tail is due to both

the longer slowing down time and the preferential absorption of power on energetic ions in the second harmonic heating scenario. In discharge 41734 the fast ion energy content is 1.5 MJ compared to 0.7 MJ in discharge 41735.

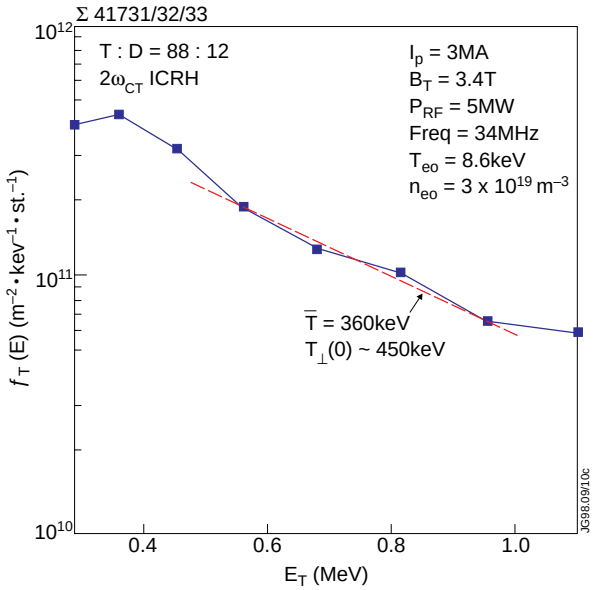

Fig. 11. Triton distribution deduced from high energy NPA measurements. The data are the aggregate of discharges with ±90°, and π antenna phasings. The line integral temperature of the triton tail is 360 keV, giving a central temperature of 450 keV.

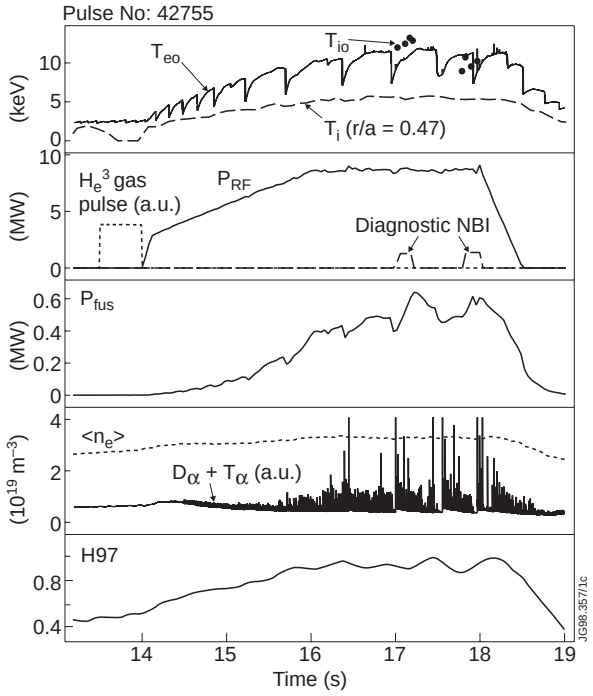

Fig. 12. Parameters of the He^3 minority ICRH discharge which generated central ion temperatures up to 13 keV. This plasma had 10% He^3 concentration, I_p = 3.3 MA and B_T = 3.7 T.

3.2 Optimised experiments.

Maximum thermal fusion reactivity was obtained from the He^3 minority heating scenario with a 45:55 D:T mixture in a 3.3 MA, 3.7 T discharge. The He^3 minority concentration was 10% and the ICRH frequency was 37 MHz at which the coupling to the plasma was near optimum. The coupled power was 8.7 MW which produced a plasma stored energy of 6 MJ corresponding to a toroidal beta of 0.9%. The fast ion stored energy was 0.7MJ and the central electron density was 3.8×10^{19} m^{-3}. Details of the discharge evolution are shown in Fig.12. An H-mode is triggered at 14.5 s and the ELMs increase in amplitude as the power is ramped up. Occasionally, a monster sawtooth crash induces a short ELM-free phase which is sometimes followed by a large amplitude ELM. The normalised confinement, H97, also increases with increasing power and reaches a value of 0.95 before the first diagnostic beam pulse. Such a value will allow ITER to ignite provided the Greenwald density can be exceeded by 10% [10] and sufficient beta can be achieved. The central ion temperature reaches 13 ± 1 keV and exceeds the central electron temperature of 11 keV. Also, the value of T_i given by the X-ray spectrometer at r/a = 0.47 is similar to that in discharge 41735 (Fig 10) implying $T_{io} > T_{eo}$. for that discharge.

As a result of the high value of T_i the neutron emission, which is entirely from thermal reactions, rises to $1.7 \times 10^{17} s^{-1}$ corresponding to a fusion power of 0.5 MW. Neutron spectrometer measurements show a Doppler broadening [8] commensurate with $T_i = 13.5 \pm 2.5$ keV in good agreement with the charge exchange measurement. Similar results were achieved with 6.5% He^3 as shown in Fig. 13 which compares the T_i and T_e profiles during the sawtooth flat top. The ion temperature profiles are noticeably more peaked than the electron temperature profiles. According to PION calculations, the ion and electron heating profiles are very similar, as shown in Fig 14, which suggests that the ion thermal transport in the plasma core is significantly less than the electron transport. This is confirmed by the TRANSP code [24] which gives $\chi_i \approx 0.6\ m^2/s$ and $\chi_e \approx 2\chi_i$ at r/a = 0.2, for example. Such values are typical of D-T ELMy H-modes in JET [25]. For the 10% He^3 case, the PION code shows that the He^3 ions take 90% of the power with 10% being deposited directly on the electrons by TTMP and ELD. Collisional power transfer from the He^3 gives 55% of the input power to the bulk ions and 35% to electrons.

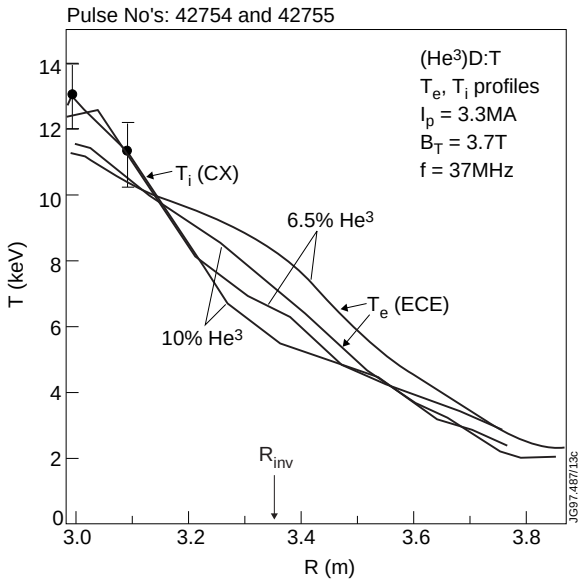

Fig. 13. T_i and T_e profiles for 6.5% and 10% He^3 minority ICRH. R_{inv} is the sawtooth inversion radius.

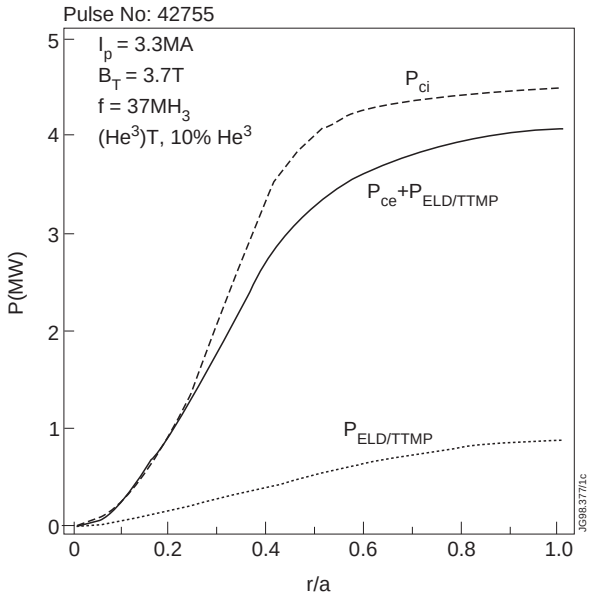

Fig. 14. PION code calculations of the power partition for 10% He^3 minority heating.

The sawteeth strongly affect the neutron emission. Tomographic reconstruction of the neutron profile monitor data shows that the plasma mixing due to the crash reduces the central emission by a factor of two. Such a reduction is consistent with the drop in central ion temperature from 13 keV to 9 keV (Fig. 12).

The PION code has been used to investigate the He^3 minority scheme for ITER [26]. The results for a He^3 concentration of 2.5% and 50 MW of power are shown in Fig. 15. The results are given in the form of contour plots of constant ion heating fraction in n_{eo}, T_{eo} space. Such a plot allows the ion heating fraction to be assessed for any choice of route to ignition. For illustration a 'direct' route from the ohmic phase (T_{eo} = 5 keV, $n_{eo} = 3.5 \times 10^{19}\ m^{-3}$) to the ignited phase ($T_{eo}$ = 35 keV, $n_{eo} = 1.0 \times 10^{20}\ m^{-3}$) is shown for which the ion heating fraction is around 70%.

The present results differ from those with He^3 added to high temperature TFTR supershots. In that case, the ICRF power is mainly absorbed by the tritons[28, 29] due to the low He^3 fraction (2%) and the high ion beta. In the $2\omega_{CT}$ scheme in JET, an optimisation of higher production (ion heating) was attempted. The central electron density was varied from 2.5 to $5\times10^{19}m^{-3}$ but better performance required operation at even higher densities. In this density range and for the available ICRH power, the discharges were sawteething which degrade performance somewhat. In general there is a conflict between ion heating and sawtooth stabilisation by ICRH. One of the best performance of the $2\omega_{CT}$ heating scheme, in terms of neutron production, is shown in Fig.16. This was a 3.3MA discharge with a toroidal field of 3.7T. The RF power was 8 MW at a frequency of 37 MHz. An H-mode is formed at 14.7s to give a normalised energy confinement, H97, of 0.7. The neutron emission rises to $2.5\times10^{16}s^{-1}$ just before the injection of the diagnostic beams for Ti measurements. The central electron temperature of 9 keV exceeds the central ion temperature of 5.8 keV. The fast ion energy content is 1 MJ which is well reproduced by calculations with the PION code. The code also predicts that 20% of the absorbed power is lost through fast tritons striking the limiters. This occurs for energies greater than 5 MeV.

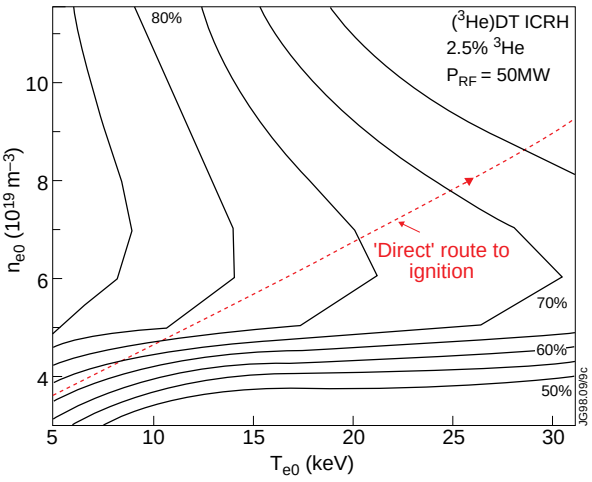

Fig. 15. Contours of constant bulk ion heating fraction for ITER parameters and 2.5% He^3 minority heating.

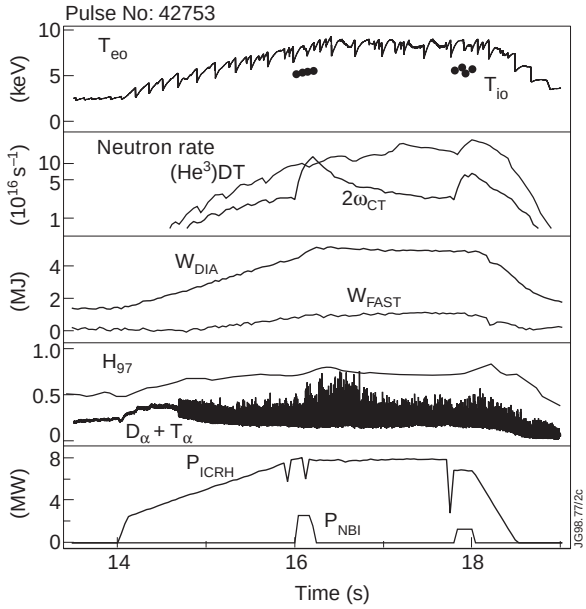

Fig. 16. Highest neutron reactivity with 'pure' $2\omega_{CT}$ heating. The neutron rate is a factor of six lower than that of a comparable He^3 minority case. Note the logarithmic scale for the neutron rate.

The power distribution calculation shows that direct electron damping absorbs 55% of the power and the tritons absorb 45%. In addition the power absorbed by the tritons is collisionally redistributed mainly to the electrons. Consequently, electron heating dominates with a total of 90% of the input power going to the electrons. The code reproduces the neutron emission, as shown in Fig. 17, including the component from the tritium diagnostic beams confirming the classical slowing down of the injected fast tritons.

Although the second harmonic tritium scheme produces mainly electron heating in JET, PION calculations similar to those in Fig 15 show that this scheme can produce mainly bulk ion heating in ITER [26]. Direct electron damping is kept low by using a value of $k_{//}$ close to 3 m^{-1}, which corresponds to ~90^{o} antenna phasing. Furthermore, two resonances are employed to give a power density of about 0.3 MW/m^3, thus reducing the energy of the fast tails, In the JET experiments the power density was ~1 MW/m^3.

The energetic tritium tail excited toroidal Alfven eigenmodes (TAE modes) which were not observed with either the deuterium or He^3 minority heating. This is qualitatively consistent with the fast ion energy content being, typically, twice that in the $2\omega_{CT}$ experiments. The trapped fast ions reach sufficiently high velocity to be in precession resonance with the modes. The TAE modes for discharge 42753 are shown in Fig. 18 to occur at a frequency between 250 kHz and 300 kHz. The frequency splitting is due to the Doppler shift for the TAEs with different toroidal numbers.

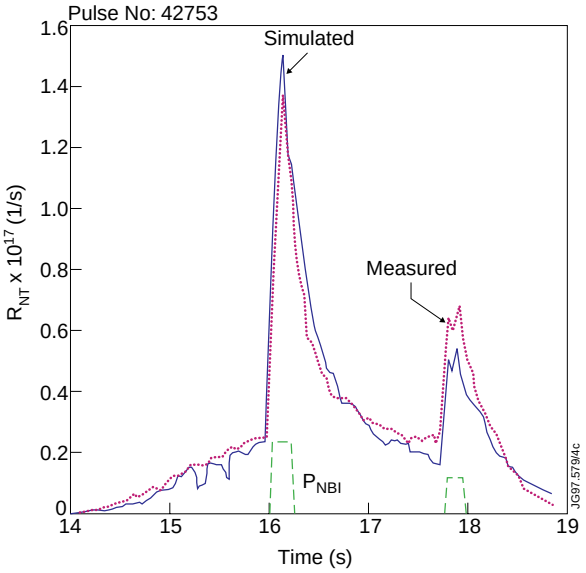

Fig. 17. PION simulation of the reactivity produced by the $2\omega_{CT}$ heating in discharge 42753.

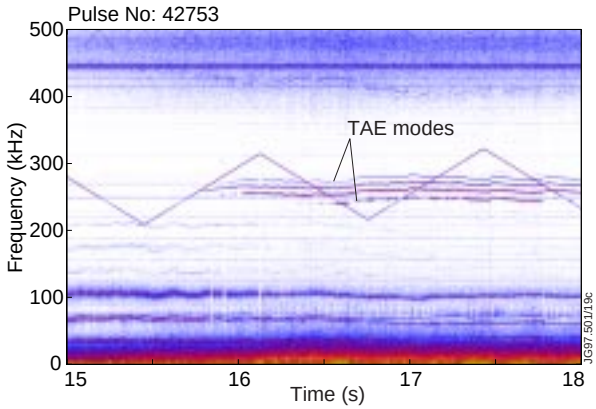

Fig. 18. Toroidal Alfven eigenmodes with frequencies in the range 250 - 300 kHz generated by fast tritons during $2\omega_{CT}$ heating. The triangular waveform is produced by the external saddle coil antenna that was used to measure stable low-n Alfvén eigenmodes throughout the experimental campaign [27].

4. TRITIUM MINORITY HEATING

The tritium minority experiments were performed with 23 MHz ICRH in 3.7MA, 3.9T discharges with tritium and deuterium fractions of 5% and 95%, respectively. The resonance layer was located at a major radius of 2.56m. This is 0.4m on the high field side of the magnetic axis and was the closest the resonance could be placed to the plasma centre; 23 MHz is the lowest ICRF frequency on JET and 3.9T is the highest toroidal field in JET so far.

In this inverted ICRH scenario, cold plasma theory places a cut-off, denoted the L cut-off [4, 30], between the resonance and the low field side antenna. In addition the ion-ion hybrid layer lies close to, and on the high field side of the cut-off. ISMENE code calculations of the positions of the cut-off and resonance are shown in Fig 19. Also shown is the fact that the R cut-off [4, 30], which, for low $k_{//}$ values, resides in the low density edge plasma, rapidly moves to the plasma centre with increasing $k_{//}$ and crosses the L cut-off for $k_{//}$ = 9.5 m^{-1}.The fast magnetosonic waves with $k_{//} > 11.5$ m^{-1} are completely cut-off. As the parallel temperature of the tritons becomes sufficient to Doppler broaden the resonance out to the cut-off, the tritons are able to absorb power from the fast wave. Calculations with the ISMENE code indicate that the tritons absorb about 65% of the power, given that the average parallel energy of the deuterons is 7 keV as determined by neutron spectrometer data. The rest of the power is absorbed directly by the electrons.

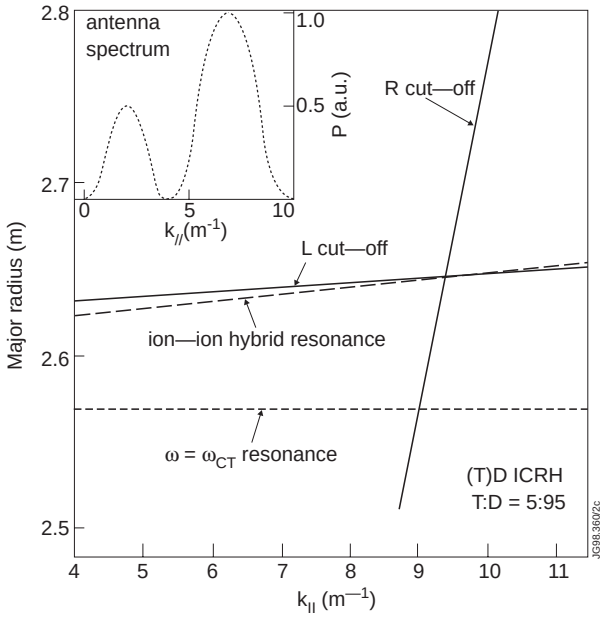

Fig. 19. Cut-off and resonance positions as a function of $k_{//}$ for the tritium minority scenario. Inset is the power spectrum coupled to the plasma at R = 3.9 m

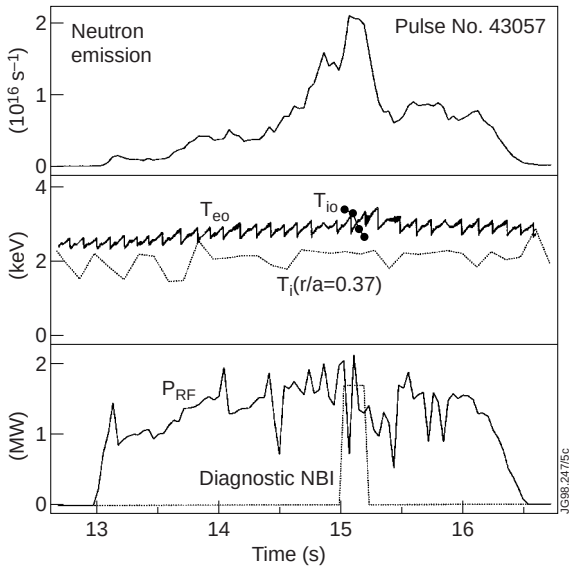

Fig. 20. Plasma parameters for the tritium minority heated discharge, 43057, which had I_p = 3.7MA and B_T = 3.87T.

The discharge evolution is shown in Fig. 20. The ICRF power from two antennas reached 1.7 MW with several trips; the antenna loading was 0.7 Ω requiring both the antennas and transmission lines to be operated at high voltage. The plasma remains in L-mode since the applied power is below the H-mode threshold. The confinement time on the ITER89-P scale [31] is 1.0 showing that the ICRF is producing good heating efficiency. The central ion and electron temperatures are both about 3.0 keV for a density of 3.5×10^{19} m^{-3}. The X-ray crystal spectrometer recorded an ion temperature of 2 keV at r/a = 0.37, close to the resonance position, consistent with the value of 2.2 keV given by the charge exchange measurement. The D-T reaction rate increases as the power is raised and reaches 1.5×10^{16} s^{-1} just before the deuterium diagnostic beam pulse. This reaction rate is about twenty times the thermal reactivity calculated

from the ion temperature and density profiles, and is due to accelerated tritons reacting with thermal deuterons. This conclusion is verified by neutron spectrometer measurements shown in Fig. 21. This spectrum was obtained by integrating over the whole discharge except during the diagnostic beams. The best fit to the data is for a triton perpendicular temperature of 35 ± 3.5 keV and a parallel temperature of 7.0 ± 3.5 keV. ICRF acceleration of tritium minority ions has also been detected in similar experiments in TFTR [32].

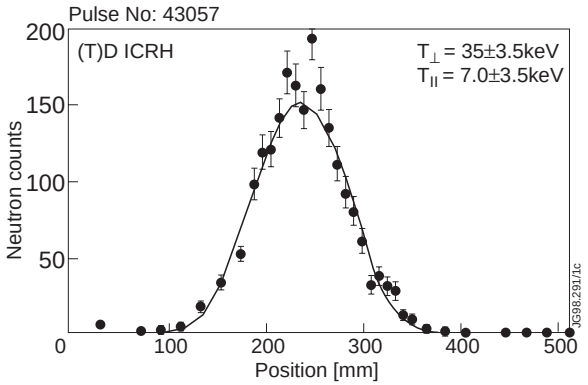

Fig. 21. Neutron spectrometer data for (T)D ICRH. The solid line is the detector response to a tritium distribution with $T_\perp$ = 35 keV and $T_{//}$ = 7 keV.

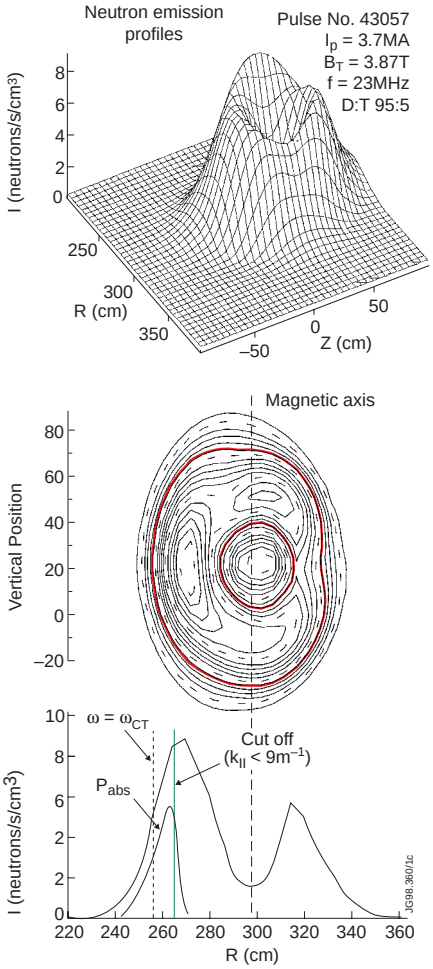

Fig. 22. Neutron emission profiles for off-axis tritium minority heating. The solid curve on the contour plot corresponds approximately to the half-height

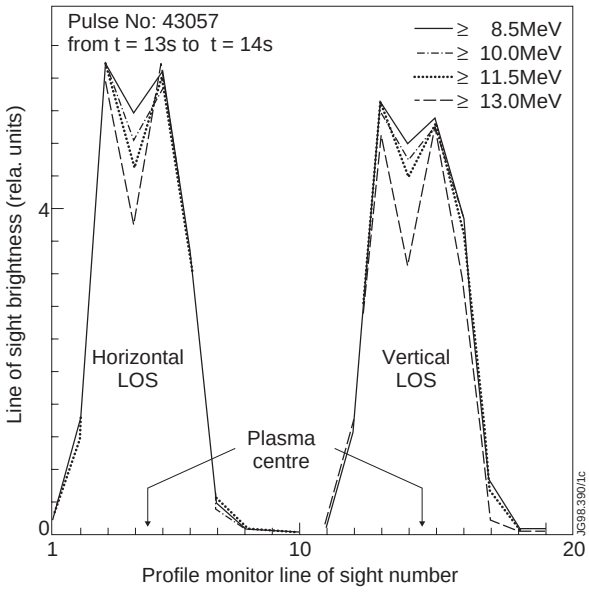

Fig. 23. Line of sight (LOS) neutron brightness for the horizontally and vertically viewing detectors of the neutron profile monitor. The hollowness of the profile increases with increasing pulse height threshold set on the NE213 scintillators. The profiles are normalised to the same peak value.

Tomographic reconstruction of the neutron emission profile is shown in Fig. 22. The best fit to the data shows an annular profile with the maximum emissivity occurring close to the peak power absorption as given by the ISMENE code. The maximum power absorption occurs near the ion-ion hybrid layer as a result of the large E_+ polarisation at this position. The asymmetry of the profile is probably due to the longer time spent by the tritons on the high field side of the magnetic axis. Orbit calculations show that 35 keV tritons close to the trapped passing boundary spend about three times longer on the high field side of the plasma centre compared with the low field side.

By varying the discriminator level on the neutron detector pulse height analysis, a coarse energy selection can be applied. The line integrated responses from the vertical and horizontal cameras are shown in Fig. 23 as this level is changed. Clearly the annular emission becomes more peaked as the neutron energy increases. This result implies that the highest energy tritons exist in a narrow annulus which broadens as they slow down and diffuse in radius. The tomography in figure 22 was made with the 8.5 MeV discriminator setting.

PION calculations, with the fraction of power absorbed by the tritium as a free parameter, reproduce the neutron emission well for an absorption fraction of 50% as shown in Fig. 24. This value is reasonably consistent with the estimate of 65% absorption by the tritons from the ISMENE code detailed above. Most of the power absorbed by the tritons is transferred collisionally to the bulk ions as shown in Fig. 25.

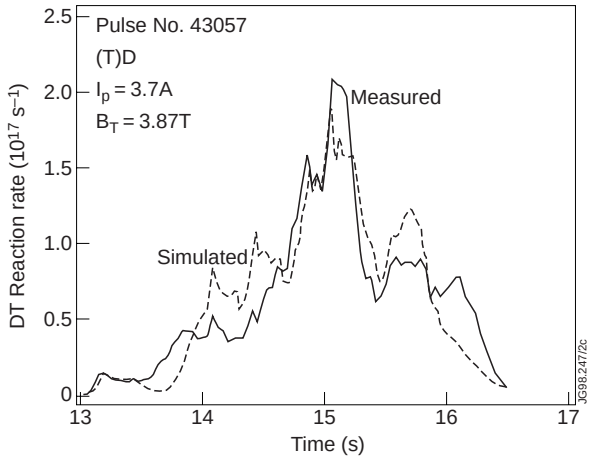

Fig. 24. PION simulation of the (T)D neutron emission from suprathermal reactions. The best fit to the data is for 50% absorption of the power by the tritons.

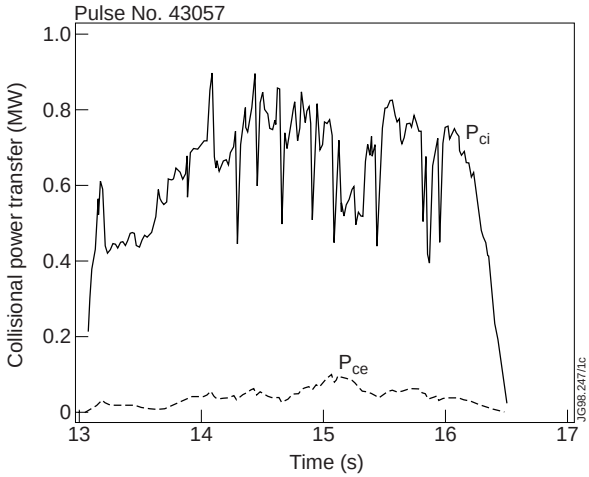

Fig.25. Collisional power redistribution of the power absorbed by the tritons. The majority of the power is transferred to the bulk ions.

5. SUMMARY AND CONCLUSIONS

The operation of the ICRF system during the D-T minority heating experiments was facilitated by the enhanced single pass damping which occurs in the scenarios studied. In particular, the He^3 minority scenario showed no evidence for cross-talk between antennas which is sometimes observed in deuterium plasmas where the damping is a factor of two lower. The deuterium

minority heating with 9% deuterium produced 1.66 MW of fusion power with 6 MW of RF power. The Q-value of 0.22 is a record for steady state discharges. This scenario also generated substantial bulk ion heating. A central ion temperature of 10.5 keV was achieved with 18% deuterium fraction. However, at this level of minority density the deuteron energy was so reduced as to indicate a transfer of power away from fast wave heating of the minority ions. The competing mechanism appears to be either mode conversion to an IBW or damping on beryllium impurities. Both mechanisms can generate the observed central bulk ion heating but definitive identification will require further D-T experiments.

The addition of a small amount of He^3 to tritium second harmonic heating is sufficient to make the damping switch completely to fundamental He^3 cyclotron absorption. Strong ion heating is produced by the He^3 minority ICRH giving ion temperatures up to 13 keV. This scheme is perhaps the most promising for ITER, for which only 2-3% He^3 is required to give 70% ion heating on the route to ignition.

The ion heating in the JET experiments is summarised in Fig. 26 which shows the central ion temperatures achieved by D and He^3 minority schemes as well the second harmonic tritium heating. Both minorities have generated ion temperatures greater than the corresponding electron temperatures but the $2\omega_{CT}$ heating gives $T_e > T_i$. This results from both highly energetic triton tail production and strongly competitive direct electron damping for the dipole antenna phasing used in the present experiments. Note also in figure 26 that the average central temperature for the best $2\omega_{CT}$ discharge falls below the trend followed by the minority schemes. This feature is a consequence of the loss of energetic tritons and the orbit broadening of the heating profiles.

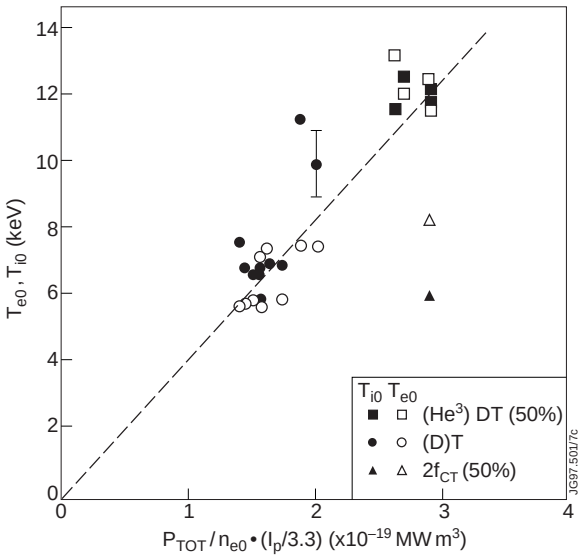

Fig. 26. Central ion and electron temperatures plotted against power per particle times I_p. The proportionality to current takes account of the scaling of confinement with I_p

In ITER, the power density can be kept below 0.3 MW/m^3 by using two resonances to spread the deposition of the 50MW input power. The energy of the triton tail will be low enough to give mainly bulk ion heating. In addition, all the fast ions will be confined and the heating will be central. The direct electron damping fraction is small if the antenna spectrum has $k_{//} \approx 3\ m^{-1}$.

All the above three heating schemes produced H-modes having small amplitude, high frequency ELMs with $\Delta W/W < 1.5\%$ which is close to the value of 1% required by ITER. The H-factors for the minority schemes, H97 ≈ 0.95, are consistent with ignition on ITER at a density 10% above the Greenwald value [10].

The inverted ICRF scheme of 5% tritium minority in a deuterium plasma has been demonstrated as a successful heating method with about 50% of the fast wave power damped by the tritons. The tritons reached an energy of 35 keV for 1.7 MW of power and the fusion reactivity was dominated by suprathermal reactions. This scheme is useful for low tritium density experiments in ITER, but requires a frequency of 29 MHz which is outside [33] the present design range (40-70 MHz).

With the exception of the high fraction deuterium minority experiments, the fusion reaction rates in all the above scenarios are precisely predicted by the PION code calculations. Such a high level of agreement gives great confidence in the predictions for predominantly bulk ion heating in reactor plasmas.

ACKNOWLEDGEMENTS

It is a pleasure to thank all our colleagues at JET who operated the tokamak, the heating systems, the tritium handling and re-processing and the diagnostics.

REFERENCES

[1] J Jacquinot et al., Plasma Physics and Controlled Fusion, 27 (1985) 1379.

[2] The JET Team, presented by J Jacquinot, 18th EPS Conference on Plasma Physics and Controlled Fusion, Berlin, 1991.

[3] B Fechner, Ph.D Thesis, Optimisation of the A2 RF Antennas for Ion Cyclotron Heating on the JET Tokamak, Universite de Provence, Aix-Marseille, France, 1996.

[4] T H Stix, Nuclear Fusion, 15 (1975) 737.

[5] The JET Team, presented by J Jacquinot, Plasma Physics and Controlled Fusion, 30 (1988) 1467.

[6] V P Bhatnagar, J Jacquinot and the JET Team, Fusion Engineering and Design, 26 (1995) 575.

[7] L-G Eriksson, C Gormezano, J Jacquinot and D F H Start, Proceedings of the Workshop on ICRF Heating and Current Drive in D-T Plasmas, Princeton Plasma Physics Laboratory, January, 1994 (Edited by J R Wilson and C K Phillips).

[8] D F H Start et al., Physical Review Letters, 80 (1998) 4681.

[9] A Kukushkin, 16th International Conference on Fusion Energy, Montreal, 1996 (IAEA, Vienna, 1997), Vol. 2, p. 987.

[10] J G Cordey et al., Plasma Physics and Controlled Fusion, 39 (1997) B115.

[11] T H Stix, Plasma Physics, 14 (1972) 367.

[12] L-G Eriksson, T Hellsten and U Willén, Nuclear Fusion 33 (1993) 1037.

[13] L-G Eriksson, Nuclear Fusion, to be published.

[14] A A Korotkov, A Gondhalekar and A J Stuart, Nuclear Fusion, 37 (1997) 35.

[15] R Majeski et al., Proceedings of the 12th Topical Conference on Radio Frequency Power in Plasmas, Savannah, (AIP 403, edited by P M Ryan and T Intrator) 1997, p. 73.

[16] G Grosshoeg et al., Nuclear Instruments and Methods in Physics Research, A249 (1986) 468.

[17] J Källne, Diagnostics for Experimental Thermonuclear Fusion Reactors 2, Plenum Press (New York), ISBN 0-306-45835-7, p. 449 and J Källne et al., Uppsala Univ. Neutron Physics Report., UU-NF 98#2 (July 1998), to appear in Rev. of Scientific Instruments.

[18] O N Jarvis, J M Adams, F B Marcus and G J Sadler, Fusion Engineering and Design, Vol. 34/35 (1997) 59.

[19] F Porcelli et al., Proceedings of 17th EPS Conference on Controlled Fusion and Plasma Heating, Amsterdam, 1990 Vol. 14B p. 327.

[20] F W Perkins, Nuclear Fusion, 17 (1977) 1197.

[21] J Jacquinot, Proceedings of the 3rd Topical Conference on Radio Frequency Plasma Heating, California Institute of Technology, Pasadena, California, 1978, paper D4.

[22] K Appert, T Hellsten, J Vaclavik and L Villard, Comput. Phys. Commun., 40 (186) 73.

[23] K D Zastrow, L-G Eriksson and E Righi, Plasma Physics and Controlled Fusion, 39 (1997) 27.

[24] G A Cottrell et al. and references therein, to be published in Nuclear Fusion.

[25] R V Budny et al., Proceedings of the 25th EPS Conference on Controlled Fusion and Plasma Physics, Prague, 1998, to be published, and private communication, 1998.

[26] D F H Start et al., Proceedings of the 24th EPS Co7ference on Controlled Fusion and Plasma Physics, Berchtesgaden, 1997 Vol 21A, Part I, p.141.

[27] A Fasoli et al., Plasma Phys. Control. Fusion 39 (1997) B287.

[28] J R Wilson et al., Physical Review Letters, 75 (1995) 842.

[29] C K Phillips, et al., Physics of Plasmas, 2 (1995) 2427.

[30] R Majeski, C K Phillips and T R Wilson, Physical Review Letters, 73 (1994) 2204.

[31] P N Yushmanov, T Takizuka and K S Riedel, Nuclear Fusion, 30 (1990) 1999.

[32] C K Phillips and R Majeski, Princeton Plasma Physics Laboratory, Princeton, NJ, unpublished data, private communication, 1997.

[33] G Bosia et al., 16th International Conference on Fusion Energy, Montreal,1996 (IAEA, Vienna, 1997), Vol. 2, p. 917.